Heliyon 11 (2025) e42294

Contents lists available at ScienceDirect

Heliyon

journal homepage: www.cell.com/heliyon

Research article

Preparation of dual mode spectroscopic system for testing: Analysis of sample holder and investigation of intensity noise

Walaa Alayed [a], Momna Ikram [b], Usman Masud [c,*]

[a] Department of Information Technology, College of Computer and Information Sciences, Princess Nourah bint Abdulrahman University, P.O. Box 84428, Riyadh, 11671, Saudi Arabia
[b] Biomedical Research Consultant, 44000, Islamabad, Pakistan
[c] Power Consultant Group, 54000, Lahore, Pakistan

ARTICLE INFO

Keywords:
Biomedical sensor
Intracavity absorption spectroscopy
Sample holder
Dual mode laser
Relative intensity noise
Cavity optomechanics

ABSTRACT

Absorption spectroscopy is combined with the principle of multiple wavelengths to develop a biomedical sensing mechanism, laid by two Fibre Bragg Gratings. It is essential to incorporate a sample holder in the setup in which the substances can be tested, necessitating its complete investigation without and with the holder, in both directions. The average losses of the fibre junctions are 0.44 and 0.18 dB, respectively, with accuracy of ±0.2 dB which lies within the intensity profile specified by the manufacturer (0.3 dB). Next, the spectral profiles and its respective factors (slope, threshold, mode spacing, intensity levels) of both systems are compared and thoroughly investigated on technical grounds, to examine any anticipated issues for the sensor's operation. Afterwards, we place the holder in the laser setup and check its efficiency by comparing it the intensity profiles of the system without it, under identical parametric values. The average Relative Intensity Noise is found to be consistently low and analogous in both setups, with scientific justifications. Repetition in the forward and reverse directions, and swapping the positions of the lenses, the outcomes show homogenous patterns, which provides conclusive approval with specified parametric regulations in this work.

1. Introduction

Analysing the gases exhaled in human breath to detect drugs is one of the newest study fields in the modern world [1–3]. By measuring the concentrations of chemicals that affect the composition of breathing gas, this is done to track, detect, and treat symptoms of sickness in people. Based on this data, it aids in the identification of possible illnesses or medication dosages in people. These molecules are known as biomarkers or volatile organic compounds (VOCs) [4–7] and reach the bloodstream. Despite the fact that over 500 distinct chemicals have been proven to be biomarkers in breath, these compounds are usually present in very tiny amounts.

Many analytical methods, including, but not limited to, advanced techniques like mass spectrometry and gas chromatography, are being actively investigated and used to identify these low amounts of VOCs [7,8]. Despite being widely used, these conventional techniques have some drawbacks that may reduce their ability to reliably identify and measure them. For example, problems with time resolution occur, leading to delays that may make the inquiry that follows more difficult. Furthermore, these techniques fre-

* Corresponding author.
E-mail address: usmanmasud123@hotmail.com (U. Masud).

https://doi.org/10.1016/j.heliyon.2025.e42294
Received 22 January 2025; Accepted 25 January 2025

Available online 28 January 2025

quently have poorer detection resolutions, which makes it difficult to discern between any related chemicals. Furthermore, detection ambiguity is a serious disadvantage since the presence of additional VOCs might skew results and cause data to be misinterpreted. Furthermore, these conventional methods might not be as sensitive, especially when detecting VOCs at incredibly low concentrations [9–12].

Considering this, absorption spectroscopy is an interesting and potentially beneficial method for VOC detection [13–15]. Using this technique, light is sent through a sample, and the interaction between the light and the molecules within the sample is examined. Researchers might make insightful inferences about the distinctive qualities of the sample under investigation by analysing how light is absorbed across particular wavelengths. In its simplest form, absorption occurs in specific wavelength ranges as a result of interactions between the molecules and the light's energy. This behaviour may indicate the concentration and presence of certain VOCs [16–18]. This technology may be able to overcome some of the drawbacks of conventional VOC detection techniques by providing significantly higher sensitivity and separating substances [19–21].

Our research aims to advance biomedical sensing technologies by investigating innovative strategies that improve sensitivity and performance through the use of laser modes and the effective implementation of optical devices [22–24]. We aspire to lay one of the groundworks for the creation of advanced biomedical sensors capable of delivering authentic outcomes across diverse pharmaceutical purposes.

2. Methodology and system details

2.1. Importance of absorption spectroscopy

The easiest way to measure how much a material absorbs is letting electromagnetic radiation of intensity $\mathbb{I}$ fall on it, thereby consequently decreasing the intensity after travelling through the material. The resulting intensity, with single pass, is the transmitted intensity $\mathbb{I}_{\mathbb{T}}$. The absorption coefficient of the tested material can be determined from the Lambert-Beer law [25].

$$\mathbb{A} = 1 - \mathbb{T} = 1 - \exp\left[-\alpha_{\mathrm{eff}} \times l_{\mathbb{A}}\right], \tag{1}$$

where $\mathbb{A}$, $\mathbb{T}$ and α_{eff} and $l_{\mathbb{A}}$ are absorption, transmission, absorption coefficient and length of the absorbing material, respectively.

Wavelength resolved absorption measurements are critical techniques used in fields like chemistry, physics, and materials science, to understand the interaction of light with matter [6,21]. Traditionally, these measurements rely on the use of a combination of a broad band light source that is paired with a subsequent monochromator. This source emits a wide range of wavelengths, and the monochromator serves to isolate specific wavelengths for analysis, thereby allowing researchers to measure the absorption properties of materials at different wavelengths.

An intriguing alternative to this conventional setup involves using semiconductor lasers which present several advantages that make them very attractive for wavelength resolved absorption measurements. One of these benefits is their narrow line width, which means that they can produce light with specific and well-defined wavelengths. This characteristic is particularly valuable to do precise measurements.

In addition, semiconductor lasers also possess excellent tunability which allows one to adjust the wavelength of the emitted light across a broad range, enabling investigations into various spectral regions. Furthermore, semiconductor lasers can have their gain characteristics tailored to match almost any desired spectral range, providing flexibility that broad band light sources cannot do not offer.

Therefore, a significant advantage of using semiconductor lasers in absorption measurements is the potential for their increased sensitivity which arises directly from the nature of the lasing process itself [9,18]. When an absorber material is integrated into the laser resonator, the interaction between the light produced by the laser, and indirectly from the absorbing material, is enhanced. In this manner, this setup can lead to a more pronounced absorption signal, facilitating the detection of even minute changes in the sample's absorption properties.

2.2. Intra cavity absorption spectroscopy in laser systems

This innovative method of incorporating the absorber material directly into the laser system is referred to as Intra Cavity Absorption Spectroscopy (ICAS), and allows for more precise and sensitive measurements, making it an appealing option for respective researchers [13,15]. The advantages of semiconductor lasers, combined with the capabilities of ICAS, position this technique as a powerful tool in the realm of wavelength resolved absorption measurements, thereby enabling deeper insights into the properties of materials after their interactions with light.

2.3. Target substances for detection and analysis

Near-Infrared (NIR) Spectroscopy is a good method for studying VOCs because it can find the absorption of light in the NIR region (about 700–2500 nm), which relates to overtones and groupings of molecular motions, especially in the C-H, N-H, and O-H bonds [22,23]. Usually, VOCs have these bonds so they can be found in the NIR range. Numerous compounds can be detected by using this technique, as shown in Fig. 1.

- Alcohols possess strong O-H stretching and bending vibrations detectable in the NIR region and visible in the NIR region.

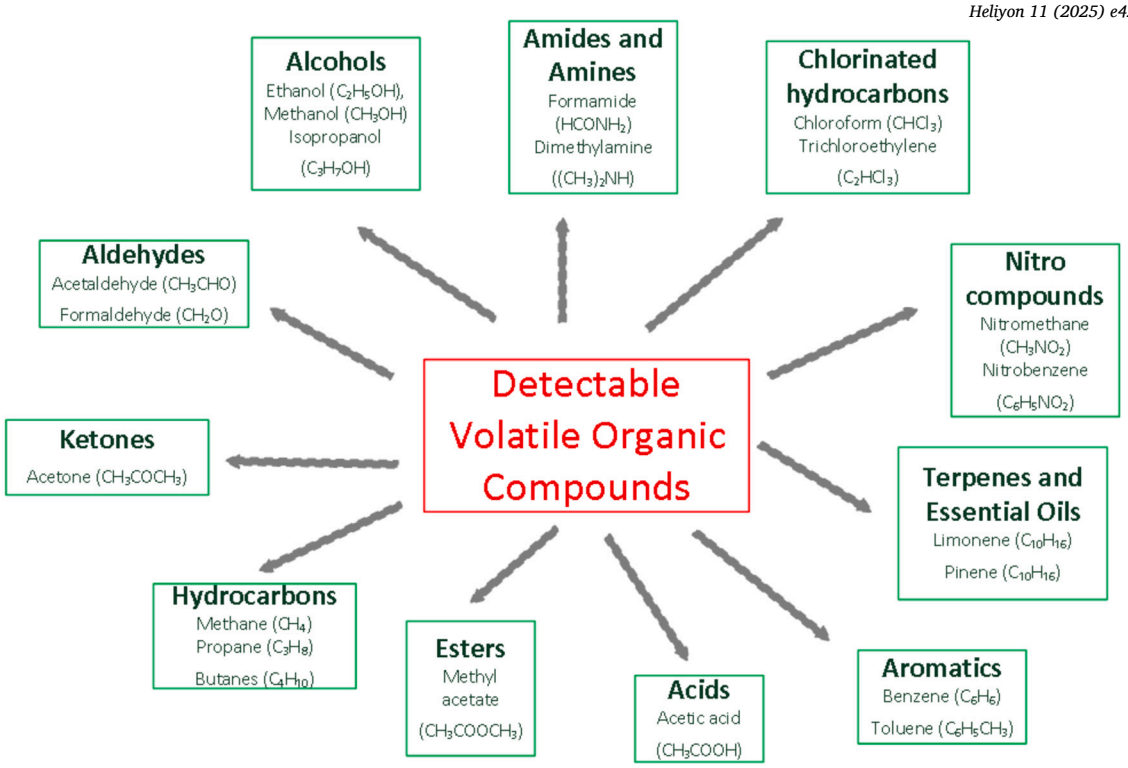

Fig. 1. Classification of the target compounds (moleculars) that can be sensed and detected with the aid of spectroscopic techniques in the NIR region (700-2500 nm).

- Aldehydes constitute characteristic C-H bonds and C = O bonds; these can be detected through their overtone bands and combination bands in the NIR.
- Ketones show strong C-H bending vibrations, detectable in NIR spectra. The O-H stretch and C = O vibrations are within the NIR range for acids.
- Aromatic compounds display characteristic C-H overtones and combination bands in the NIR spectra.
- These bonds characteristic absorption bands can detect compounds containing multiple C-H bonds in Terpenes and Essential Oils.
- Specific overtone and combination bands associated with functional groups are useful for identifying nitro compounds.
- Chlorinated hydrocarbons arise from C-H stretch modes, and in some instances, halogen-related vibrational modes, in the NIR.
- Chlorinated hydrocarbons may also be detected, particularly based on N-H stretching and bending vibrations.

Generally, NIR spectroscopy detects these VOCs due to the ability of the method to reveal molecular vibrations involving bonds such as C-H, O-H, N-H, and C = O which are typical for organic compounds. It is a method that can be applied in environmental analysis, quality control, and industrial applications for real-time monitoring of VOCs. We prepare our experimental system with the aforementioned technique for alcoholic compounds, namely Proponol and Acetone after thorough calibration.

2.4. Improvement in sensitivity of the laser system

An improvement of sensitivity in ICAS in comparison to the traditional single-pass method can be attributed to two primary mechanisms [12,20], each contributing significantly to performance.

Firstly, we have the *resonating phenomenon.* This effect arises from the ability of the system to intensify the absorption signal through multiple passes of the active material within the resonator structure. In essence, light interacts repeatedly with the sample, leading to an increased absorption signal. This amplification is beneficial as enables the detection of lower concentrations of analytes that might otherwise be undetectable with a single pass of light through that sample. Importantly, this resonating phenomenon operates independently of mode interaction. This means that it can increase sensitivity regardless of the specific ways in which different modes of light within the resonator might interact with each other.

Secondly, and significantly more impactful on sensitivity, is the fact known as *mode competition.* This becomes particularly pronounced in systems with strictly homogeneous broadening of gain, which is a condition where the gain profile stays uniform across the range of frequencies being measured. In these circumstances, the competition between different modes of light present within the cavity leads to a more pronounced amplification of the desired absorption signal. This interaction results in a dramatic increase in sensitivity, making it the key operational principle underpinning the advancements described in this work. By leveraging the inter-

play of mode competition, the ICAS technique can attain sensitivity levels that surpass those available through conventional methods, enabling more precise measurements in various applications.

In this way, the combined effects of the resonating phenomenon and mode competition fundamentally transform the sensitivity landscape of ICAS, providing substantial advantages over traditional single-pass methods and pointing it out as a powerful tool for analytical applications.

2.5. Introduction to experimental system

The system being studied incorporates an exclusive lasing mechanism which comprises a Semiconductor Optical Amplifier (SOA) together with its controller, the Laser Diode Controller (LDC). This is shown in Fig. 2a [26,27].

The key operation of the system starts with the production and amplification of light which is generated by these two devices. This light output goes to two components which are called Fibre Bragg Gratings (FBGs). These gratings are therefore differentiated as FBG_i and FBG_o, to distinguish them as being incorporated in the inner and outer cavities, respectively.

The placement of these FBGs is very important for the operation of the system since they select and reflect certain frequencies and do not allow the others to pass through. The light is hence controlled in a certain way. The output of the system is taken out from the coupler in between these two FBGs, as shown in the figure, and goes to the Optical Spectrum Analyser (OSA) [29]. The output spectrum can thus be seen and analysed on this device in detail.

Besides the optical measurement device, the output light is also coupled to an electrical measurement system as described in [30–32]. This dual measurement capability is very important as it will enable the assessment of all the parameters of the system in a more technical manner and thus determine both optical and electrical characteristics of the system at the same time.

The electrical measurement system consists of a Photodiode, which converts it to the electrical equivalent, followed by a Bias-Tee and Low Noise Amplifier (LNA) [6,14]. This set of equipment helps not only in the detection of electrical signals, but also the Relative Intensity Noise (RIN), an important parameter that aids in a deeper understanding and application of the system [36,37,32]. This is depicted in Fig. 3.

In addition, isolators are used within the configuration to maintain the integrity of the measurements and prevent feedback of light. These isolators perform an essential role in preventing any light that tries to reflect back into the SOA and relevant instrumentation as illustrated in the figure. Not only does this feature provide protection to delicate system components, it also improves system reliability and stability of the experimental output.

2.6. Current work

In essence, the method showcases a robust combination of optical and electrical measurements using FBGs and isolators to ensure advanced optics and insight into lasing application. As the system targets the detection of substances, we plan to place a glass cuvette in the existing system. This will help us in placing the substances which must be tested and analysed. It is of utmost importance to highlight at this level that the prospective glass cuvette should exhibit such properties that do not interfere with the existing system's characteristics, which would cause complications in the output performance at a later stage [21,33]. Therefore, the analysis and investigation of the glass cuvette and the system becomes mandatory, before proceeding with any measurements with the fluids, which becomes the pivotal point of this work. The system's behaviour with respect to numerous conditions is analysed, and a detailed comparison is made with the holder and without the glass cuvette, accordingly.

The purpose of this work is to check the performance of the existing system after incorporating the glass cuvette,[1] where the substance of interest can be inserted and tested afterwards. For this purpose, we resort to the principle of ICAS [15,34,35]. In other words, the holder is placed inside the laser's cavity that directly boosts the sensitivity of the system, as shown in Fig. 2b. In this way, the achieved results are much more accurate as compared to the situation where the holder is placed outside the cavity of the laser, thereby anticipating the goal of a biomedical sensor for human breath.

3. Investigation of sample holder

The holder is placed inside the laser cavity (2b). To understand and check the operation of this component inside the laser resonator, this component is characterized and examined for errors beforehand. We have chosen the synthetic Quartz glass cuvette with 2 polished sides that has septum screw caps, keeping into account the requirements of our setup and testing [38–40].

This holder features two polished sides that have been optimized for the purpose of absorption spectroscopy and two frosted sides for a firm grip. The quality of the polished surfaces can be maintained using traditional optical cleaning methods. However, since this cuvette only has two polished windows, it is specifically designed for absorption related experiments, and is unsuitable for fluorescence spectroscopy, as per vendor recommendations.

Built with an extended resistance to chemicals, this cuvette can hold a maximum substance upto 3.5 ml. Its outer periphery is 12.5 mm^2, allowing a length of 10 mm for light to pass through the substance. There is a PTFE septum screw cap with each cuvette that creates makes it air-tight, thereby stopping any mixture of inside material with that from the outside. A needle can be pierced

[1] Referred to as *holder* from now on, for the sake of convenience.

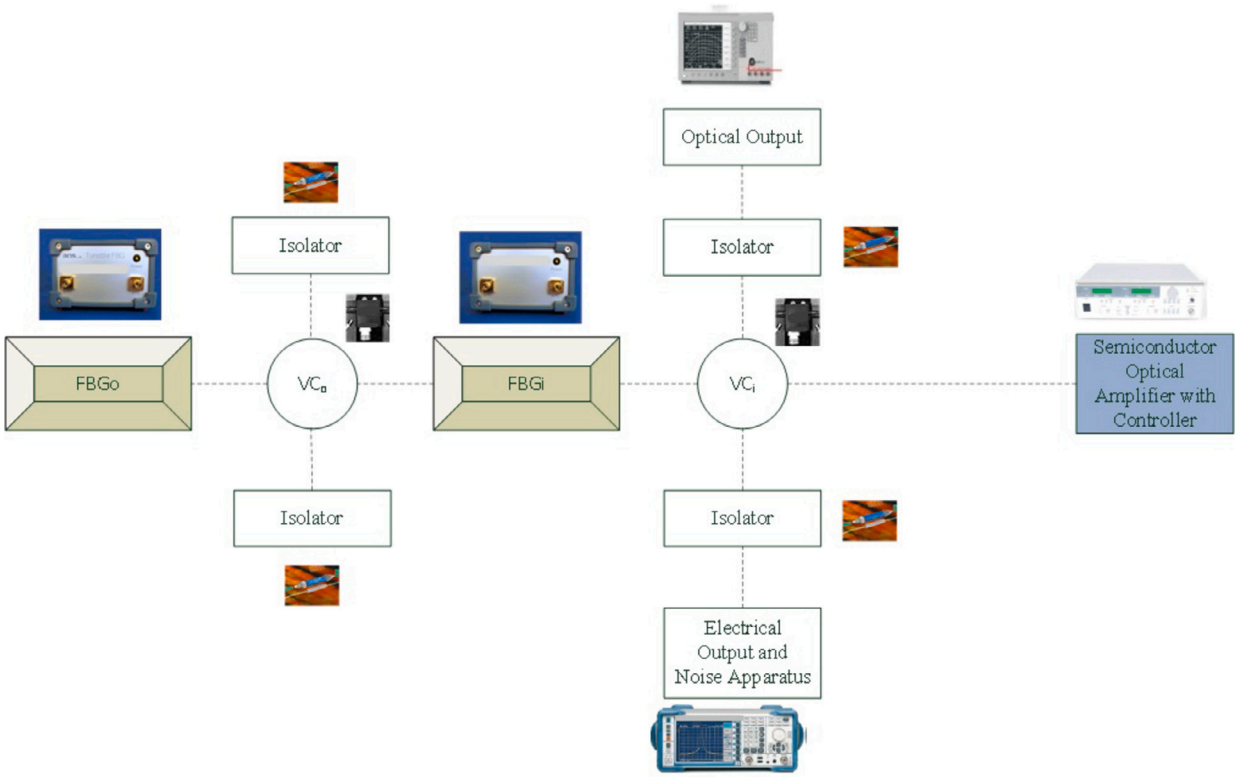

(a)

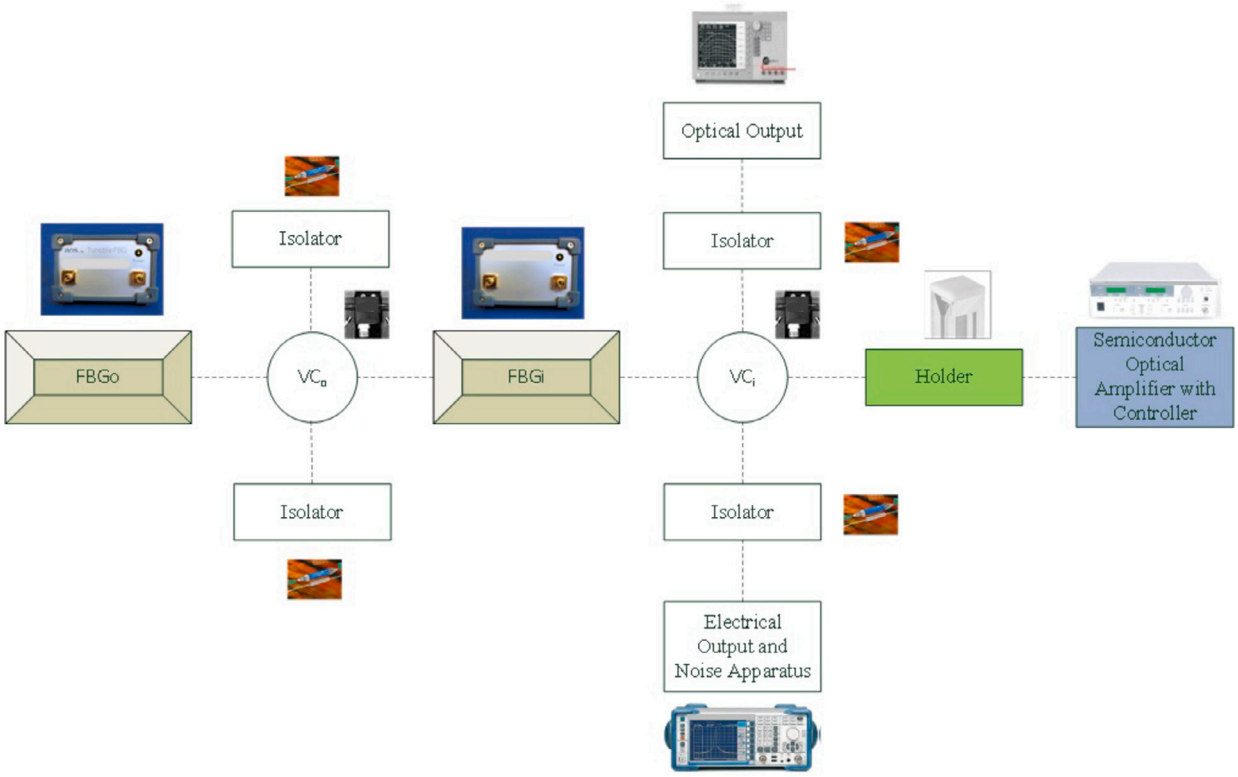

(b)

Fig. 2. Experimental setup containing the SOA, LDC, FBGs, isolators, VCs, along with the output devices. (a) without the Holder, and, (b) with the Holder.

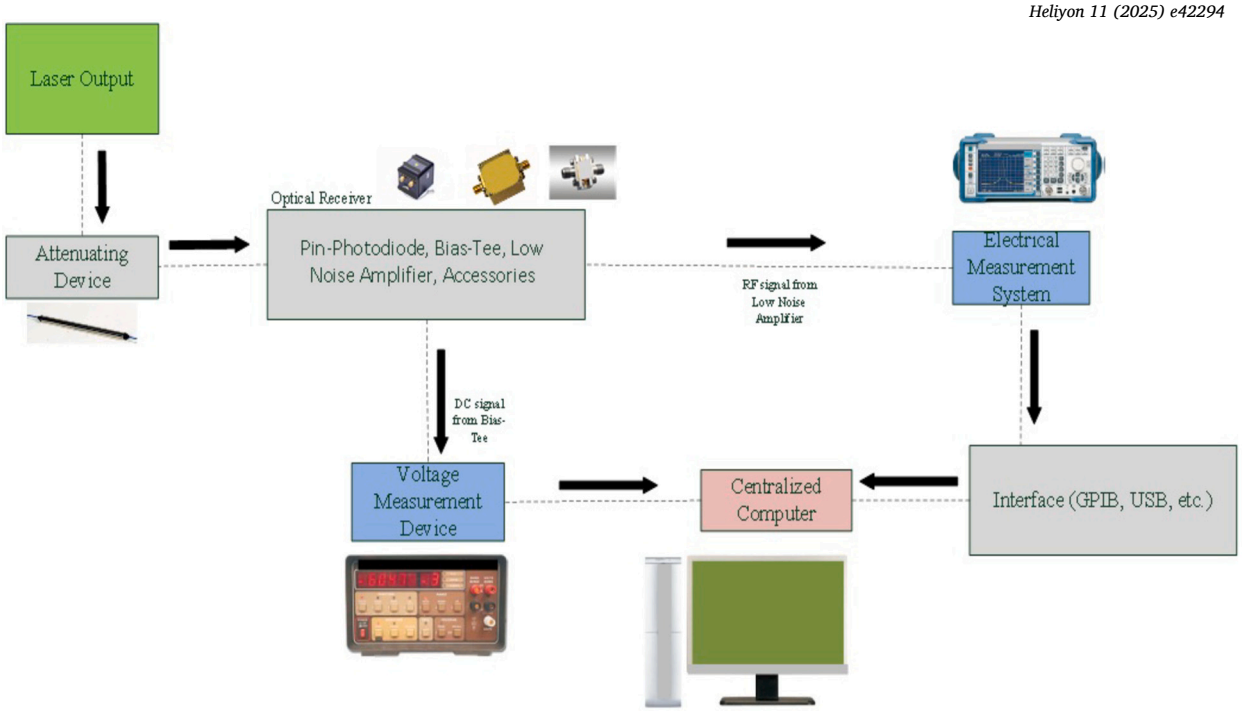

Fig. 3. Illustration of the optical receiver and supporting devices that are used for the calculation of RIN of the said system.

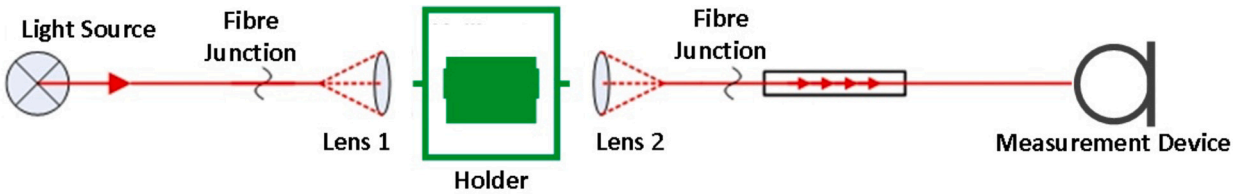

Fig. 4. Measurement setup for characterizing the collimation optics.

from the above to break this seal. In this way, the device offers maximum protection of the substance under test both from outside and inside.

The next sections explain the methodology used for the characterization and the measurement setup for this purpose. This is followed by the evaluation of the recorded data.

3.1. Procedure of the characterization

The characterization of the holder consists essentially of a different technique. A reference (standard) measurement of the intensity is recorded without the presence of the holder. Afterwards, the holder is inserted, and the intensity is measured again. The former value of intensity is subtracted from its latter value. The resulting difference and an average splicing error of the fibre junction can be used to estimate the loss of intensity caused by the installation of the holder. The results obtained in this manner are then compared with the manufacturer's specifications.

3.2. Measurement setup

To do the characterization procedure, a special experimental setup is designed to measure the intensity losses. Fig. 4 shows the path of light from left to right to characterize the holder. The optical path begins with a light source. Since this light source should have a high intensity within a wide wavelength range, an Edge-Emitting Light Emitting Diode (EELED) is used here [41–43]. It has a high intensity in the wavelength range from 1500 nm to 1600 nm and is therefore well suited for measurements.

The EELED is connected to the holder via a single mode fibre. Here, the light passes through the first lens (lens 1) that amplifies and ensures a straight flow. The second lens (lens 2) collects the light and couples it into the fibre. From here, the light passes through an isolator which lets its flow in the forward direction and is then detected by the OSA.

Table 1
Maximum intensity values of the fibre junctions at a wavelength of 1536.2 nm.

Fibre Junction	Value
Fibre junction 1	-42.62 dBm
Fibre junction 2	-42.53 dBm
Fibre junction 3	-42.27 dBm
Fibre junction 4	-42.34 dBm

Integrating the isolator enables a direct connection to the OSA. Light reflections that can occur due to the design of the OSA and fibre connectors are absorbed by the isolator. They are therefore no longer coupled into the holder and can be neglected in technical considerations, since the ratio of the intensity of reflections is very small as compared to the intensity of the incident light.

To record the measured data, the OSA is set to a fixed wavelength range with the marker at the position of the maximum intensity. In this way, the marker allows us to directly measure the intensity losses.

3.3. Measurement method for the characterization

The holder is measured in two different directions (both forward and reverse). These are arbitrarily chosen terms that are only given this name to distinguish them. The measurements are carried out in both directions to ensure that there is no preferred direction for installation in a laser resonator.

Thus, the holder can be tested in two directions, between the light source and the spliced isolator. The positions of the splice junction are shown in Fig. 4. A special method is used for splicing, known as the *intensity controlled splicing* [44,45].

Intensity-controlled splicing is a method used in optical fibres or photonic devices when the light transmitting power level must maintain a certain value and vary accordingly to achieve desired performance throughout the fibre optic splice stages. In comparison, traditional splicing is where the fibres come together, but in intensity-controlled splicing, it's about keeping or enhancing light strength where those two lengths of fibre become one. This is especially important in applications like telecommunications or data transmission where signal integrity matters.

The approach could involve modifying splicing conditions like temperature, pressure or alignment in order to keep the light output intensity above defined levels [46,47]. They need to minimize the loss signal so that there is less power overdoses through free space, and hence our optical system can run more effectively.

Using this method in our system, the glass fibre section of the holder is spliced *visionless* at one end of the glass fibre. Visionless here means that no information can be obtained about intensity losses at the splice point. The purpose is simply to connect the holder to the isolator on one side. The loose end of the glass fibre can be spliced in a controlled way. The opposite fibre ends are not yet connected to each other, and they rather guide the light to the OSA. In this way, an intensity value can be measured that is maximized by precisely adjusting the fibre ends. The fibre ends are only spliced together when the maximum achievable intensity value is obtained. In the next step, the blindly created splice junction is removed and replaced by another splice point created in a controlled manner. The first fibre junction is thus used as a *reference* for the second fibre junction, thereby providing a relative value of the intensity loss due to the installation of the holder. This procedure is carried out once for each fibre junction for both the forward and reverse directions, respectively.

3.4. Procedure for experimental data

Measurements are made through the whole wavelength range from 1500 nm to 1600 nm by the EELED. This EELED has a characteristic curve with a maximum value in this wavelength range. This maximum value is present at a wavelength of 1536.2 nm with an intensity profile of -41.7 dBm. The holder should not change the curve in any form when installed in the system, rather it will only attenuate (lower) the intensity of light. Moving through the splice junction, the damped intensity peaks are identified with markers and used as reference points for the intensity control mechanism of the splices. From the marker positions, the data could be determined as shown in Table 1.

The numbered splice junctions in Table 1 show different intensity profiles. The numbering here again provides the order of the intensity control mechanism of the fibre junctions. There are namely two of these fibre junctions for the forward and reverse directions, i.e., (1) and (2) apply to the forward direction, whereas, (3) and (4) to the reverse direction, respectively. The entire process is then repeated by swapping the positions of the lenses. This was done to ensure the accuracy of the obtained results, which are presented in Table 2.

3.5. Evaluation of measurement data

The procedure provided above results in four intensity spectra, two for each measurement direction (i.e., forward and reverse).

The intensity values given in Tables 3 and 4 were determined from the maxima of the curves in Figs. 5 and 6, respectively. In order to determine the loss of intensity because of the installation of holder, the measured intensities in Table 1, I_{S_n}, are subtracted

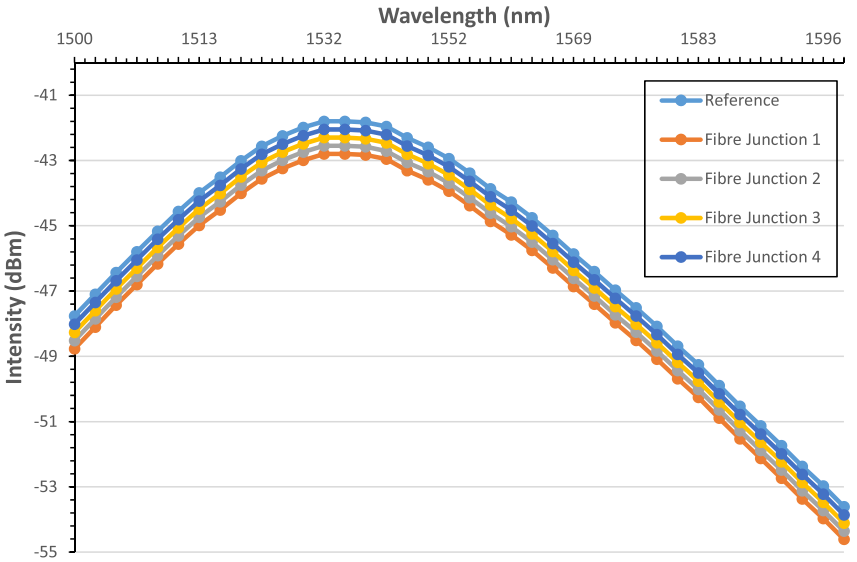

Fig. 5. Graphical representation of the measured spectra (reference and fibre junctions 1-4).

Table 2
Maximum intensity values of the fibre junctions at a wavelength of 1536.2 nm, after swapping the lenses.

Fibre Junction	Value
Fibre junction 1	-42.63 dBm
Fibre junction 2	-42.59 dBm
Fibre junction 3	-42.33 dBm
Fibre junction 4	-42.32 dBm

Table 3
Difference in values of the fibre junctions in the forward and reverse directions (w.r.t. Fig. 5).

Fibre Junction	Value
Fibre junction 1	0.85 dBm
Fibre junction 2	0.76 dBm
Fibre junction 3	0.49 dBm
Fibre junction 4	0.57 dBm

Table 4
Difference in values of the fibre junctions in the forward and reverse directions (w.r.t. Fig. 6).

Fibre Junction	Value
Fibre junction 1	0.83 dBm
Fibre junction 2	0.73 dBm
Fibre junction 3	0.53 dBm
Fibre junction 4	0.54 dBm

from the reference values of intensity I_{measured}. This difference in the intensities δI, gives us a value which includes the relative splice junction error that occurred during the installation procedure, i.e.,

$$\delta I = I_{\text{reference}} - I_{\text{measured}}. \tag{2}$$

As part of a series of measurements, an average error of 0.32 dB was determined for splice points at the laboratory. If this value is included in the analysis of the intensity loss, the value of average loss for the forward and reverse directions $Loss_{\text{average}}$ is 0.44

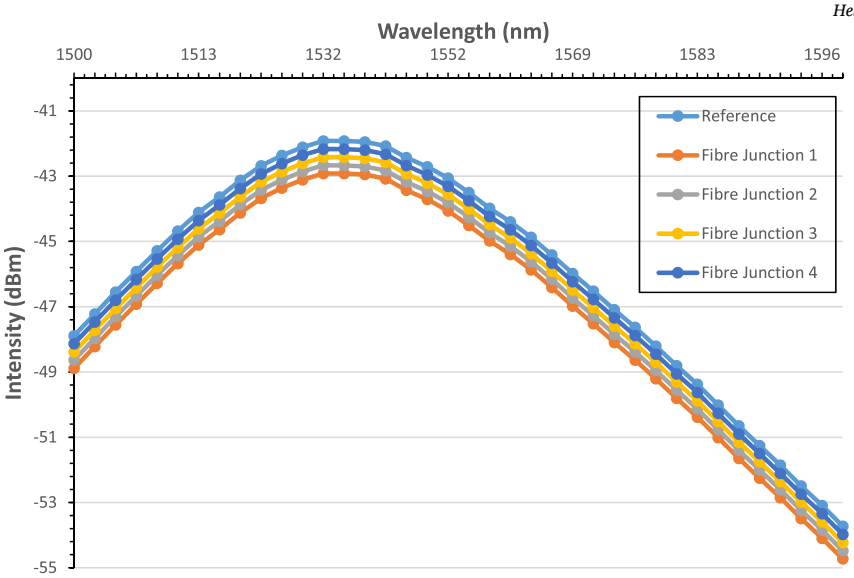

Fig. 6. Graphical representation of the measured spectra (reference and fibre junctions 1-4).

dB and 0.18 dB, respectively. The manufacturer's prescribed value of the intensity loss due to installation is 0.3 dB (independent of direction) and can be confirmed by characterization. As a result, the average losses $Loss_{\text{average},1}$ and $Loss_{\text{average},2}$ are found with an accuracy of ± 0.2 dB, a value which certainly lies within the intensity profile specified by the manufacturer, i.e.,

$$0.3 > \begin{cases} Loss_{\text{average},1} \\ Loss_{\text{average},2} \end{cases} \tag{3}$$

Therefore, the holder can be used regardless of the direction of its placement during the experimentation. The intensity values only vary with the quality of the splice junctions.

4. Comparison of results

It is imperative to check the performance of the system after inserting the holder with the system that had been earlier present without it [32,24]. For this purpose, the system's parameters are adjusted as per previous work, and the experimentation was repeated (Figs. 2b and 3).

4.1. Investigation of spectral tunability

The investigation is carried out under conditions with standard operating conditions, i.e., SOA temperature of 15 °C, 20 °C, 25 °C and 30 °C, and injection current of 125 mA. To ensure uniformity in the experimental setup, the FBGs are first aligned at the same temperatures. The temperature of FBG_i is kept at 23 °C while that of FBG_o is kept at 32 °C.

In order to fine tune the output modes of the system, temperature of FBG_o is raised to 62 °C. This adjustment is to enable a thorough investigation of thermal impact on mode characteristics. After the heating process, FBG_o is slowly brought back to its initial temperature of 32 °C. This cooling is in small steps of 1 °C, so as to display how alterations in temperature affect the system's performance.

After each step of heating or cooling it is crucial to use VC_o to bring the mode intensities to a state of equilibrium for the measurements. This step is important for consistency. When the stabilisation is complete, spectral data is acquired. To minimize the effect of noise in the measurements, each spectral reading is averaged over 30 measurements. This averaging is done to ensure that the data collected is accurate and represents properly the behaviour of the system under the examined thermal conditions. The final spectra are shown in Figs. 7, 8, 9 and 10, and then stored for further processing.

- *Pattern*
  It is seen that the intensity levels of both modes show a similar pattern without the holder and with the holder, regardless of the direction of the lenses. This means that the newly added device does not play any role in the pattern of the spectrum, which is a significant fact for the sensor.
- *Slope*
  One of the foremost parameters to understand the pattern of the graph is to analyse its slope and compare it with that of the earlier setup. To understand this, we have to understand the underlying phenomenon.

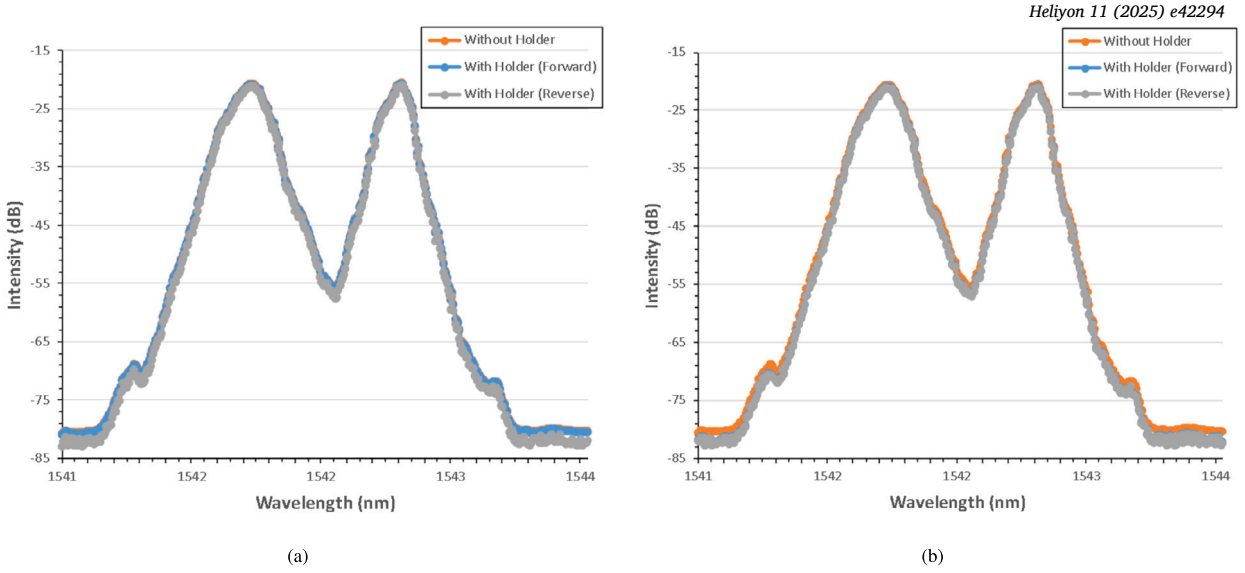

Fig. 7. Comparison of system behaviour with the earlier system with SOA@15 °C, FBG_i@1542.01 nm and FBG_o@1542.51 nm. The results without the holder and with the holder are respectively shown in (a) and (b), before and after swapping the directions, and lenses.

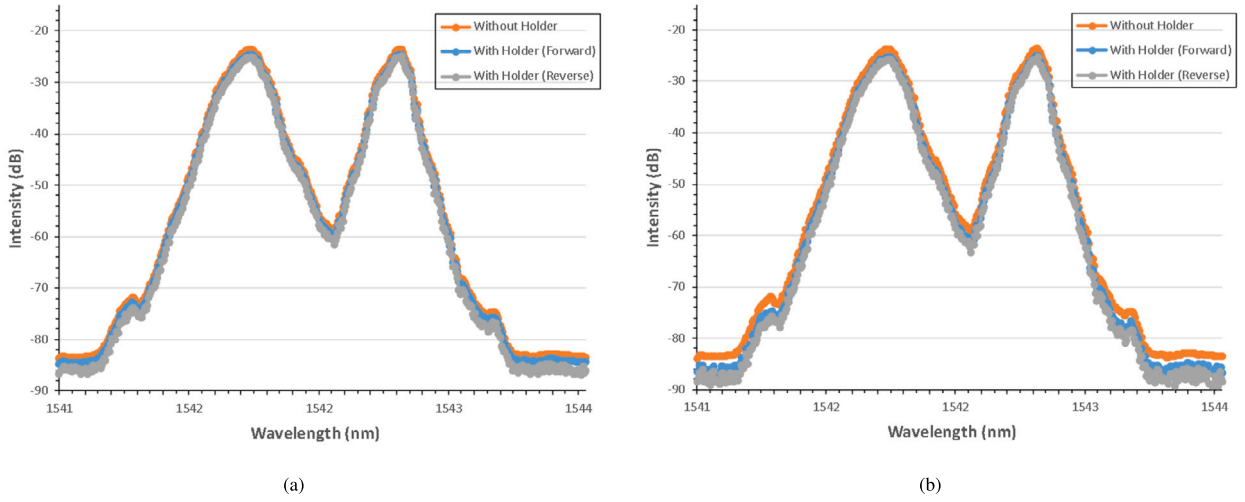

Fig. 8. Comparison of system behaviour with the earlier system with SOA@20 °C, FBG_i@1542.01 nm and FBG_o@1542.51 nm. The results without the holder and with the holder are respectively shown in (a) and (b), before and after swapping the directions, and lenses.

The tuning response to the heating of FBGs is calculated for both systems. The tuning mechanism, detailed in [6,32], remains unchanged. As a result, the slope that indicates the tuning response for FBG_o is very similar in both systems. However, there exists an offset between the two responses, which can be attributed to a relaxation effect caused by the adhesive used to bond the FBG to the heated aluminium blocks.

When the aluminium blocks are heated, the glue that secures the FBG also undergoes heating. It is likely that, despite the manufacturer's specifications suggesting otherwise, the glue does not maintain its mechanical stability under the influence of heat [28,26,39]. This condition leads to slight relaxation of the fibre during each heating cycle. The repeated cycles of heating and cooling that occurred between the measurements reported by our work in late 2023 and the recent system established in early 2024 have resulted in observable changes in the offset of wavelength tuning that can be achieved through thermal adjustments. Table 5 summarizes the parameters of the linear regressions that were applied to the data displayed in Figs. 7, 8, 9 and 10. This data shows how changes in material behaviour have affected the system's performance over time and gives a concise summary of the relationships revealed in the data gathered from both systems.

- *Mode Spacing*

An analysis of figures shows that the mode spacing between the two modes has been successfully retained. In the earlier system without the holder, the mode spacing was found to be 0.5±0.01 nm, and the same value has been obtained for the current system

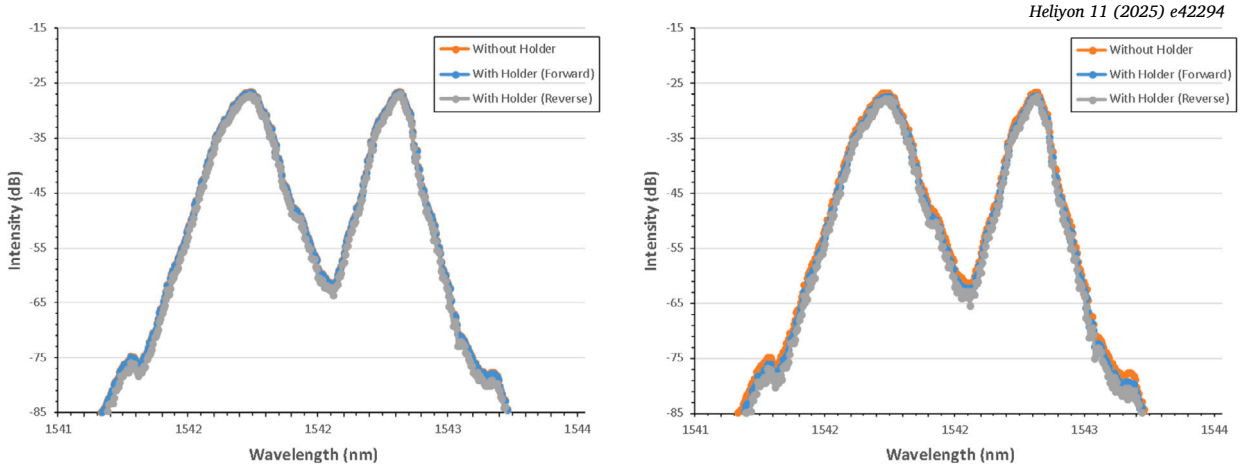

Fig. 9. Comparison of system behaviour with the earlier system with SOA@25 °C, FBG_i@1542.01 nm and FBG_o@1542.51 nm. The results without the holder and with the holder are respectively shown in (a) and (b), before and after swapping the directions, and lenses.

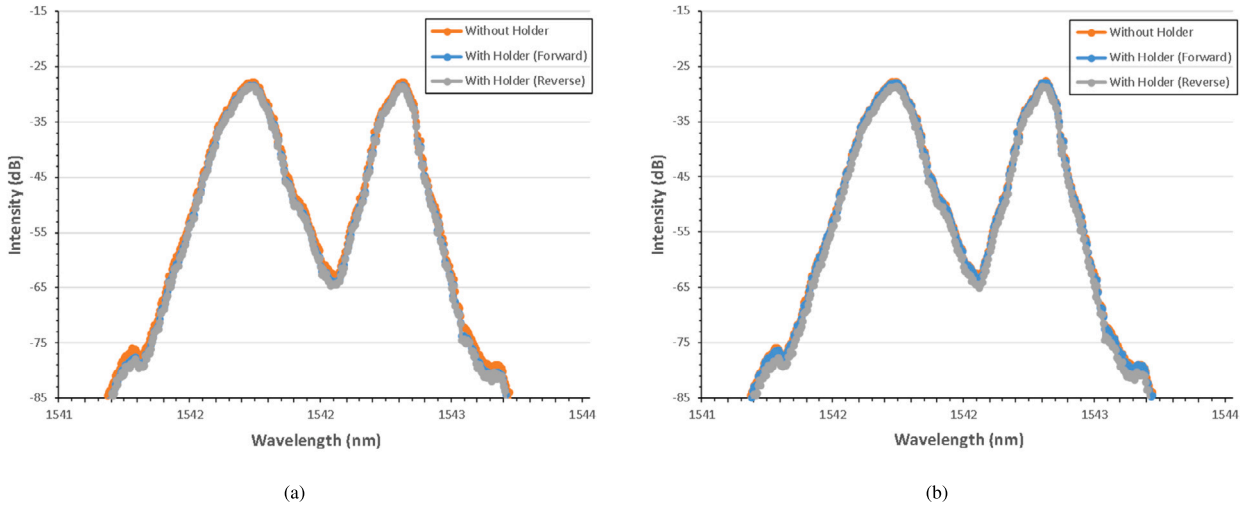

Fig. 10. Comparison of system behaviour with the earlier system with SOA@30 °C, FBG_i@1542.01 nm and FBG_o@1542.51 nm. The results without the holder and with the holder are respectively shown in (a) and (b), before and after swapping the directions, and lenses.

Table 5
Results obtained after linear regression of the earlier setup and current setup.

No	Experimental Setup	Value of y-Intercept (nm)	Slope (pm/°C)
1	**Earlier Setup**	*1541.448±0.007*	*32.3±0.2*
2	**Current Setup**	*1541.461±0.007*	*32.2±0.2*

with the holders. This sustains the accuracy of the results once the sensor is put into operation, as the distance between both wavelengths is integral to the entire sensor concept underneath, in correlation with mathematical analysis in [54,55].

- *Intensity Levels*

It is important for a biomedical sensor to find the lowest amount that can be detected with its existing system. For our setup, this implies analysing the intensity level existing between both modes that would correlate to that amount. For instance, we see from Fig. 7a and 7b that the intensity level between both modes at the time of their existence reaches a minimum of 32.5 and 32.3 dB, respectively. This means that any difference in the absorption spectrum of any substance that lies in this wavelength regime can be successfully detected up to this intensity level. Similarly, the other values of the minimum intensity difference when both modes are present at their highest levels, are shown in Table 6.

Table 6
Difference of each mode's maximum intensity with the point of least intensity existing between both modes FBG_i and FBG_o.

No	SOA Temperature (°C)	Minimum Intensity Difference of FBG_i (dB)	Minimum Intensity Difference of FBG_o (dB)
1	*15*	*32.5±0.5*	*32.3±0.5*
2	*20*	*38.2±0.5*	*38.5±0.5*
3	*25*	*37.6±0.5*	*37.4±0.5*
4	*30*	*37.5±0.5*	*37.8±0.5*

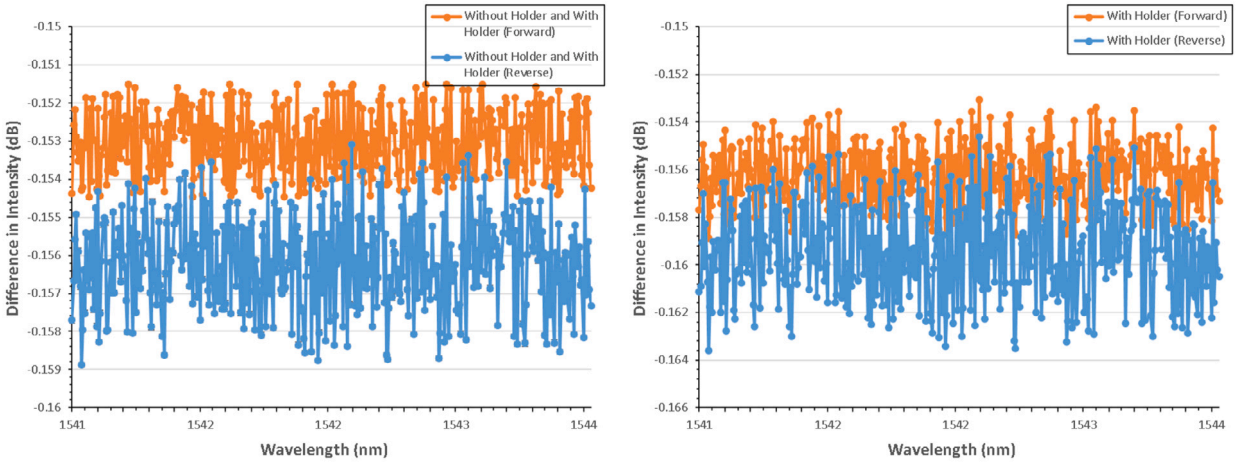

(a) (b)

Fig. 11. Difference of spectral intensities with the earlier system. The results without the holder and with the holder are respectively shown in (a) (corresponding to Fig. 8a) and (b) (corresponding to Fig. 8b), before and after swapping the directions, and lenses.

4.2. Difference in spectral intensities

The intensity levels of both modes show a minute difference in intensity before the modes start to establish their equilibrium. This happens in particular in the wavelength range of 1541.01 to 1541.05 nm. As per discussion with the technical team, this happens as a result of many quantum-mechanical effects, and are inherent to absorption spectroscopy [13,14,18,39]. For our purpose, the important thing is to see this competition when both modes establish their equilibrium state. Therefore, we resort to check the difference in spectral intensities before and after the placement of the holder in the experimental system.

The differences between the spectral intensity levels are shown in Figs. 11, 12, 13 and 14. It is seen that the difference between the intensity levels when the holder is placed in the forward direction and reverse direction, has a maximum level of -0.202 dB. This is a remarkable result, as the holder should have a minimum effect on the inherent properties of the experimental setup.

As already stated regarding vendor specifications, the holder must not have a loss of more than 0.3 dB in the system. This is crucial to the system's performance as the devices which are producing light, and the ones which are letting it pass, should be able to establish a certain level of intensity and phase that enables us carry out our experimentation. Therefore, it is desirable to put a holder in the system that has a minimum impact on the existing gadgetry.

Moreover, the holder was placed in both forward and reverse directions, and the results we cross checked. This is essential to see as to if the newly added device shows any deviation from the specifications, in order that additional technical procedures might be implemented beforehand. However, the figures show that the value ranges from about -0.153 dB at 15 °C and 20 °C to -0.202 dB at 20 °C and 25 °C. The difference in values between the former (15 and 20 °C) and latter (20 and 25 °C) temperatures is tantamount to strong mode competition at higher values of temperature which is a common fact in the analysis of systems with multiple modes, a characteristic of cavity optomechanics [51,56].

This investigation confirms that the tuning mechanism has been effectively maintained. It shows a strong ability to establish a stable intensity balance between M_i and M_o. This stability is achieved regardless of variations in the parameters of the laser system. For the sensor system, this kind of dependability is essential. It guarantees that there will not be any technical ambiguities in the system's operation. Accurate measurements and reliable performance depend on this operational clarity. The sensor system's overall efficiency and dependability are improved by its capacity to maintain equilibrium in shifting circumstances, which makes it an essential part of its intended applications.

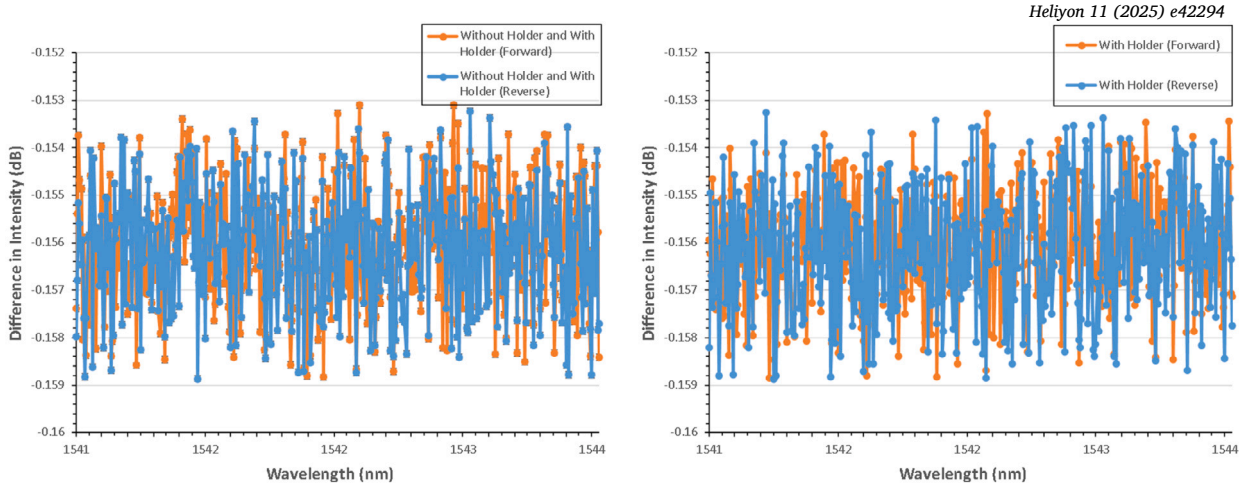

(a) (b)

Fig. 12. Difference of spectral intensities with the earlier system. The results without the holder and with the holder are respectively shown in (a) (corresponding to Fig. 8a) and (b) (corresponding to Fig. 8b), before and after swapping the directions, and lenses.

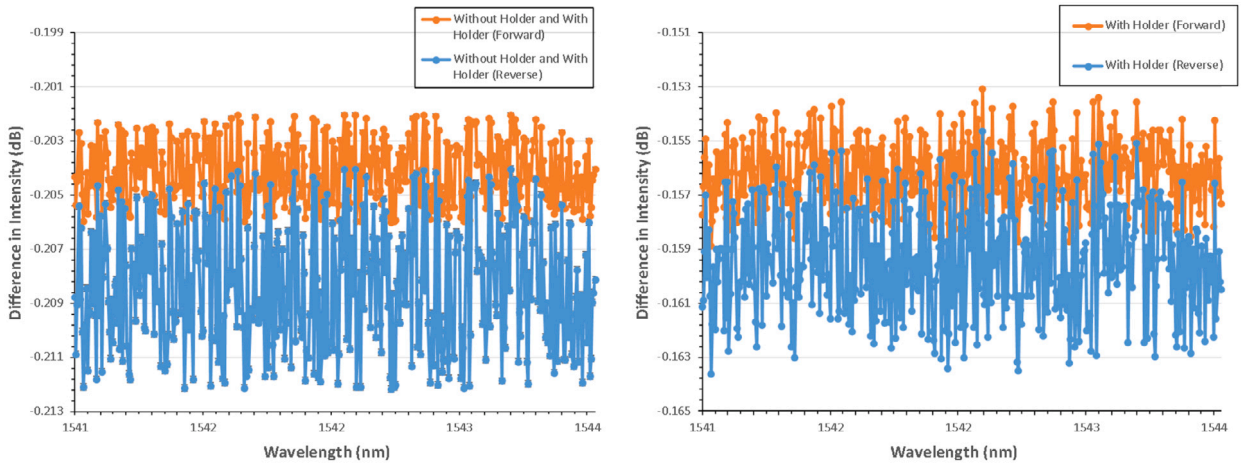

(a) (b)

Fig. 13. Difference of spectral intensities with the earlier system. The results without the holder and with the holder are respectively shown in (a) (corresponding to Fig. 9a) and (b) (corresponding to Fig. 9b), before and after swapping the directions, and lenses.

4.3. The impact of intensity noise on system performance

RIN is used to characterize the sensor output short-term fluctuations in measured intensity [48,49]. It is defined as the ratio of the power spectral density of the fluctuations to the square of average intensity. Usually, these fluctuations are seen at different frequency components and could result from many things, including laser noise, shot noise of the sensor or associated electronics, or environmental disturbances. RIN spectrum analysis gives a useful realization of dominant noise mechanisms, valuably applicable to optimization of sensor performance or design. Mathematically [20,21],

$$\mathrm{RIN}(f) = \frac{N(f)}{G_A P_L B}, \tag{4}$$

and the phenomenon along with the terms involved can be explained [31,16].

1. The measured amount of laser intensity noise, $N(f)$, is the remaining noise after subtracting contributions from dark noise and shot noise. This value of noise is analysed with the help of an Electrical Spectrum Analyzer (ESA) with a resolution bandwidth of B. It is important to understand that the ESA essentially decomposes the time-varying electrical signal from the photodiode into its frequency components, allowing us to analyse the noise power distribution as a function of frequency, f. The ESA has a key parameter known as its resolution bandwidth, B, which represents the frequency range over which the noise power

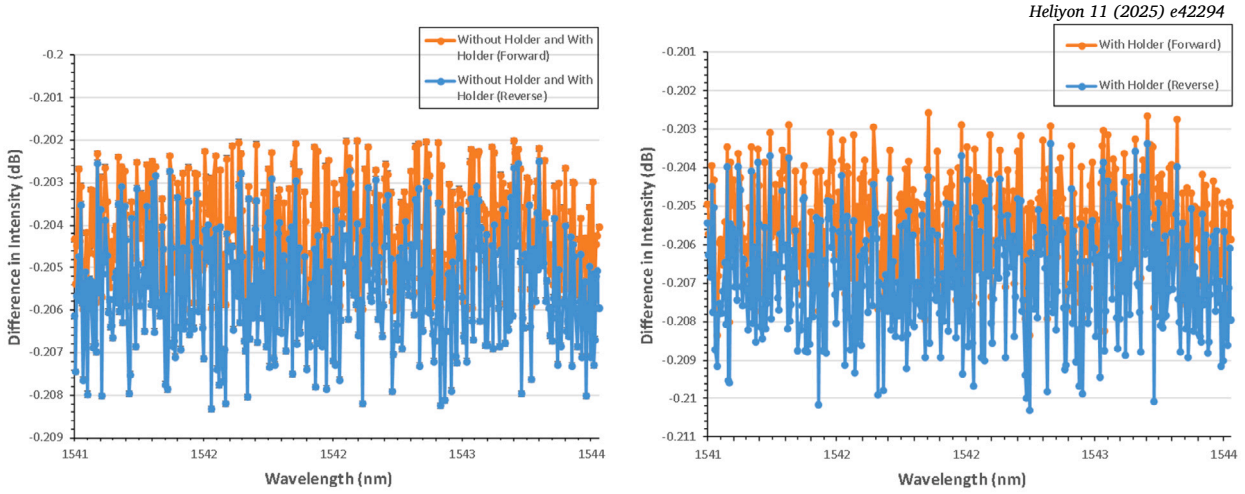

(a) (b)

Fig. 14. Difference of spectral intensities with the earlier system. The results without the holder and with the holder are respectively shown in (a) (corresponding to Fig. 9a) and (b) (corresponding to Fig. 9b), before and after swapping the directions, and lenses.

is averaged during a measurement. This bandwidth influences the apparent measured noise level, with a smaller bandwidth, thereby providing higher frequency resolution but potentially revealing less reliable noise level estimates.

2. The photodiode's signal is often quite weak and requires amplification before being examined by the ESA. This is accomplished by using a preamplifier with a known gain factor of G_A. This gain factor is the ratio at which the preamplifier enhances the incoming signal's voltage. Crucially, the preamplifier provides its own noise, which is normally and carefully described to ensure that the final results are not skewed. Furthermore, the average power measured at the photodiode's load resistor, represented as P_L, is an important metric. The load resistor is often a particular resistance that transforms photodiode current to measurable voltage. This average power, coupled with the photodiode responsiveness, is critical for determining the root mean square (RMS) level of the laser's output.
3. Besides analysing the electronics, we also have to characterize the laser light itself, by wavelength and by its spectral properties. An OSA is used to do this which measures the spatial distribution of optical power in the laser output as a function of the wavelength. This describes the spectral stability of the laser and any unwanted optical sidebands that may be present.
4. The entire measurement system is controlled and automated using the LABVIEW software which is a graphical programming environment. It not only allows us to control all the instruments (ESA, OSA), but also manage the data acquisition process from both the electrical and optical instruments. The communication between the PC running LABVIEW and these instruments is achieved through a GPIB (General Purpose Interface Bus) connection [52]. This standardized digital interface enables the computer to send commands, retrieve data and control the various instruments during the data acquisition process.

Thus the experimental measurements derived from this process are precisely captured using a suite of sophisticated instruments. These include, the Digital Multimeter (DMM), employed for measuring electrical parameters like voltage, current, and resistance; the OSA, which analyses the spectral content of light signals such as wavelength and power; and the ESA, utilized to examine the frequency domain characteristics of electrical signals. To facilitate data acquisition, these instruments are interconnected via a digital GPIB connection, a standardized interface that allows seamless communication of devices with computer systems. The acquired measurement data is then digitally recorded and saved for subsequent analysis. Finally, the data acquisition process, as well as instrument control and manipulation, is managed by LABVIEW, a graphical programming environment, specifically version 21.0.1 [29].

4.4. Dynamics between laser output and optical receiver performance

The optical receiver is one of the important elements of optical communications networks, and therefore we use it in our setup [14,24]. Generally speaking, it serves as a transducer, which converts energy from one form to energy in the other form. The focus of the optical receiver is converting the transmitted optical signal, the carrier of encoded information, to a more convenient electric signal. As the latter can be easily processed with the help of subsequent circuitry and thoroughly analysed, so the information source can be easily extrapolated out of this signal.

The primary building blocks of an optical receiver are the following.

1. *Optical Detector* This component is responsible for the initial conversion of the incoming light into an electrical current. When photons of light impinge upon the detector, they generate electron-hole pairs, thereby creating current proportional to the

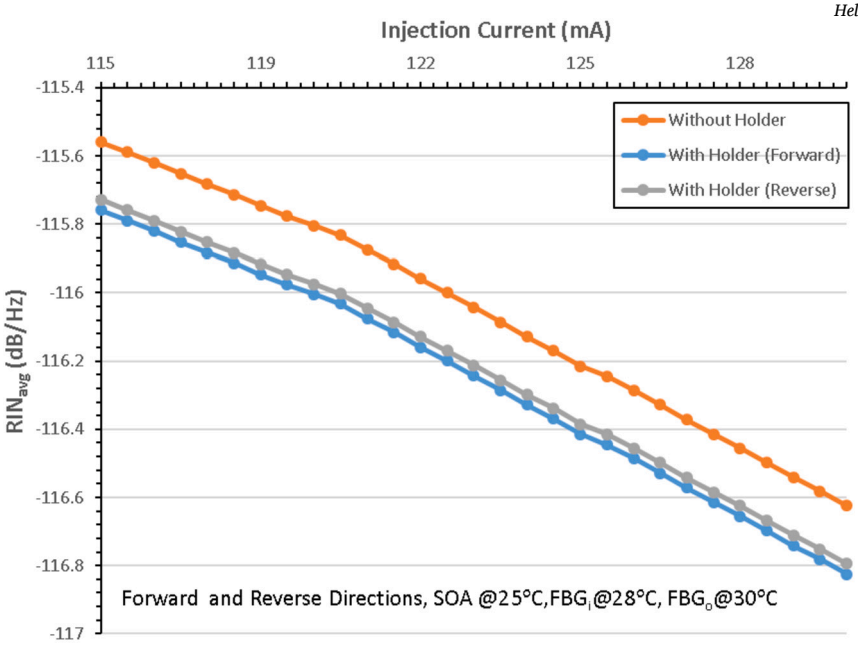

Fig. 15. Variation of average RIN with injection current (outer mode being suppressed), with lenses in normal position.

intensity of the received light. The performance of the optical detector, including its sensitivity and speed, is critical for overall system performance.

2. *Low-Noise Amplifier (LNA)* As the electrical signal generated by the optical detector is typically very weak, so the LNA's role is to amplify this weak current or voltage to a more usable level. Crucially, it does this while adding minimal additional noise to the signal. The LNA's characteristics, such as gain, bandwidth, and noise figure, significantly impact the quality of the received signal.

4.5. Experimental framework and evaluation

A temperature of 25 °C has been established for SOA. The VC_o is adjusted to suppress the exterior cavity mode in order that the internal cavity mode remains fixed at 1542 nm. With a 5 mA step, measurements are made between 115 mA and 130 mA for the input current. Afterwards, the related optical spectra and average RIN are plotted and displayed in Figs. 15 and 16, with the lenses in normal and swapped positions, respectively.

1. Figs. 15 and 16 show that when injection current increases, the average RIN reduces. The scientific reason behind this emerges from the mathematical relationship between the two quantities. The RIN of the laser goes down as the injection current goes up [50,51]. If the injection current, threshold current and output intensity are I_{inj}, I_{th}, and P, respectively, one way to express the connection between RIN and injection current is as follows [52]

$$\text{RIN} \propto \left(\frac{I_{\text{inj}}}{I_{\text{th}}} - 1 \right)^{-3}, \tag{5}$$

$$\text{RIN} \propto P^{-3}. \tag{6}$$

These formulas hold true for low bias levels, meaning that the value of RIN changes inversely with P^3 [51,53] when the lasing phenomenon is maintained further beyond the value of the threshold value of current.

2. The laser is operated well over the threshold level of the injection current in order to obtain measurements. After setting a 15 mA bias level difference, the average RIN drops by just an amount of 1 dB. Consequently, as the injection current rises, the value of the system's RIN drops. The pace of this reduction relies heavily on the current which is given to the diode laser. Larger increases in current will generally lead to a more rapid reduction in RIN, as the laser operates closer to its optimal performance point. This observation clearly demonstrates that the behaviour of our laser setup, including the impact of the components such as the holder on beam quality and stability, is not arbitrary. Therefore, we can state with certainty that the behaviour of our lasing setup in the presence of the holder is in complete scientific correlation with the intricate level of physics [19,22] which governs the underlying system, dictated by eq. (6), and therefore serves as a predictive framework for understanding the relationship between the injection current, the laser's internal dynamics, and ultimately, the stability of the output beam, for both modes.
3. The same reason applies to the fact that the values of average RIN are less after inserting the holder in the system. After exchanging the positions of the lenses, it is observed that the value of RIN in the setup with holder and lenses in forward position is slightly

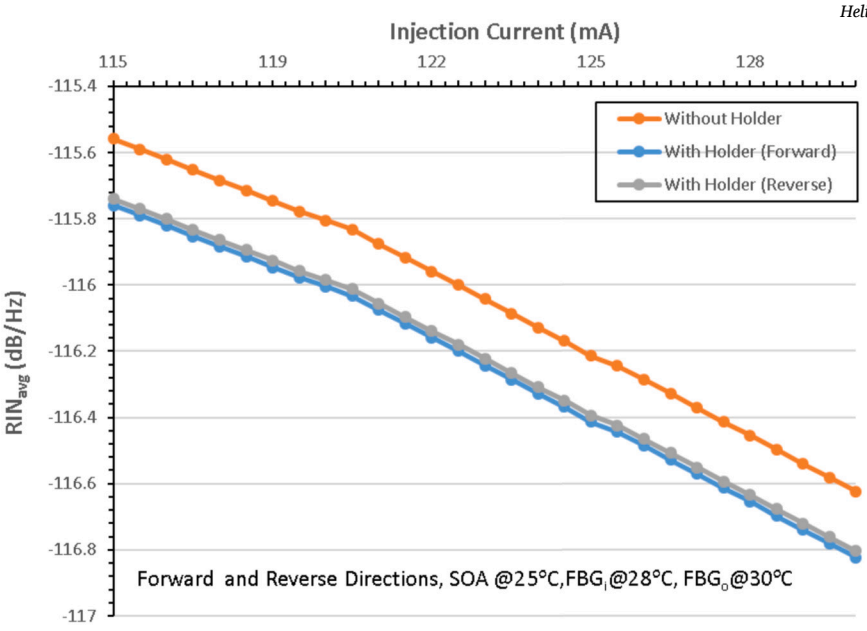

Fig. 16. Variation of average RIN with injection current (outer mode being suppressed), with lenses in swapped position.

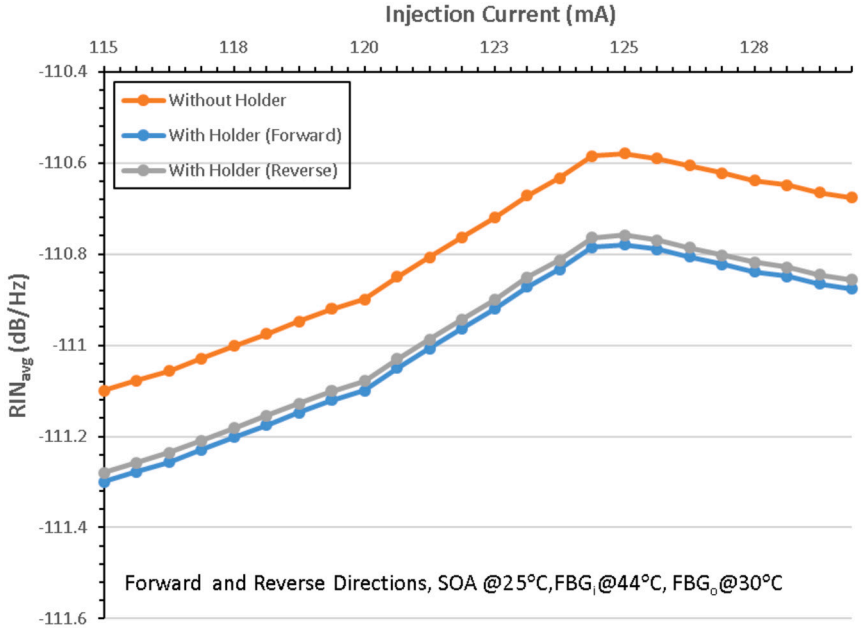

Fig. 17. Variation of average RIN with rising values of temperature and injection current, with lenses in normal position.

greater that with the lenses in the reverse position. This nominal difference amounts to an average value of about 0.005 dB, and is due to the quantum mechanical effects within the frame of cavity optomechanics [6,23,51]. Although the exact reasons of this phenomenon cannot be ascertained at this level, yet, however, this does not anticipate to have any significant effect on the results of our measurements.

4. It is noticed that as the injection current and the output intensity rise, the value of average RIN rises accordingly, as seen in Figs. 17 and 18. If we see equations (5) and (6), this phenomenon seems to be in contrast with them. However, a closer look can lead to correct scientific interpretation. At first glance, the discrepancies may seem significant, leading to potential confusion regarding the underlying principles at play. However, if we take a moment to delve deeper into the details and nuances of the equations, we can uncover a more accurate scientific interpretation. It is worth mentioning that single mode solitary diode lasers can be described by the said formulas [50,51]. Though these formulas can accurately describe the performance of single-mode solitary diode lasers, yet they are not limited to idealized scenarios. This indeed does signify their practical applicability and

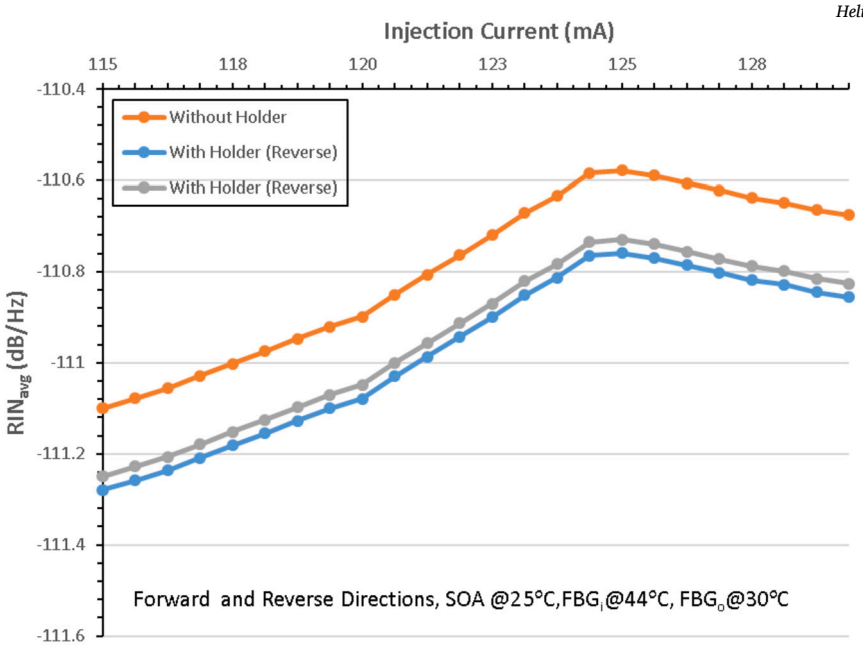

Fig. 18. Variation of average RIN with rising values of temperature and injection current, with lenses in swapped position.

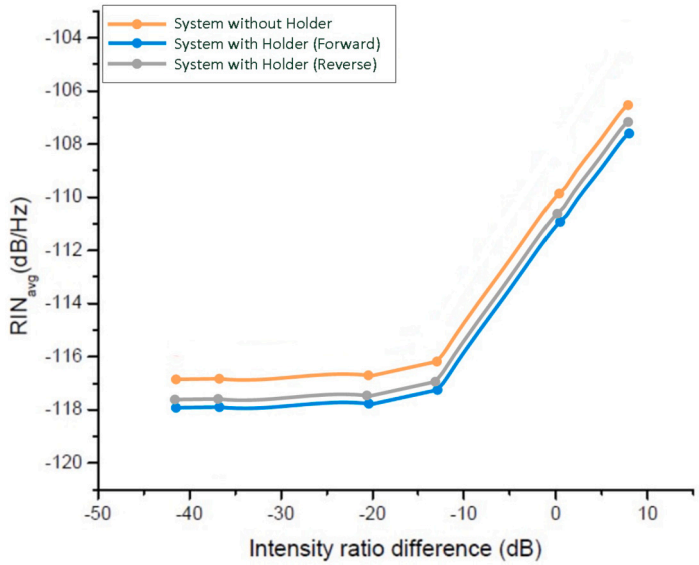

Fig. 19. Comparison of average RIN for old and new setups, lenses in normal positions.

robustness in characterizing these commonly utilized laser sources. On the other hand, we are having a system with dual modes [6,32].

5. In other words, the dual mode lasing system is described to be functioning like a single mode device (again, in this specific working state), with an outer cavity providing us a feedback mode [54,55]. Although it possesses two potential lasing modes, within this specific working state, one mode dominates, effectively mimicking single-mode operation. The 'dual-mode' designation arises from the system's structure: the external or outer optical cavity plays a critical role by providing feedback that shapes and stabilizes the primary lasing mode. This external cavity essentially functions as a feedback loop, selectively reinforcing the desired mode and suppressing others. This means that our sensor system must behave and perform differently. As a result, our laser behaves substantially different when compared to a typical single laser diode, and provided with increasing values of input current.
6. With the increase in optical feedback within the experimental setup, the impacts on the performance metrics are clearly noticeable across both configurations being studied. This observation has been visually represented and further detailed in Figs. 19 and 20. These figures illustrate how the average RIN values fluctuate under different conditions. The accompanying figures clearly

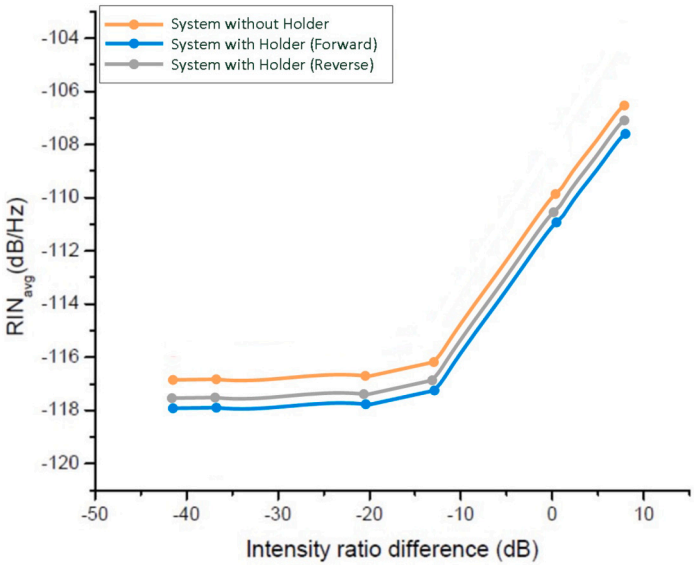

Fig. 20. Comparison of average RIN for old and new setups, lenses in swapped positions.

demonstrate how the average RIN values vary, depending on numerous influencing conditions, and understanding them is crucial for the sensor operation. Notably, this variation in RIN can be associated to an offset or balancing act akin to a direct current (DC) adjustment, where perturbations in the light intensity exhibit a systematic shift in relation to the established baseline [56,58]. As RIN quantifies how much the light's power deviates from its average value, so it is a way to measure these short-term perturbations, and highlighting the origins of this systematic shift is crucial in diagnosing and solving practical problems in experimental setups like this one.

7. Moreover, the intensity noise values at rising frequencies exhibit similar trends in both setups, suggesting that there are common underlying mechanisms at play despite the differing configurations. This trend highlights the robustness of the observed phenomena across varying experimental frameworks, emphasizing the importance of understanding the dynamics of optical feedback [57].
8. Another intriguing aspect that emerges from this investigation is the change in Relaxation Oscillation Frequency (ROF) in response to the optical feedback [58]. This behaviour is particularly noteworthy as it exhibits antagonistic trends between the two systems being examined. In our specific system, the addition of feedback causes the ROF to shift towards the right along the frequency axis, indicating an increase in frequency. In contrast, the Agilent system responds oppositely, displaying a movement of the ROF to the left, which represents a decrease in frequency.
   This divergence in ROF behaviour underpins the necessity of a nuanced exploration of the effects of optical feedback—showcasing how it can lead to significantly different outcomes based on the specific configuration and characteristics of the systems in question. Such findings not only enrich our understanding of optical feedback phenomena but also have practical implications for optimizing system performance in optical applications.

4.6. Precision constraints of intensity noise measurements

Multiple factors are present in this situation which explain the observed discrepancy in RIN estimation between our setup and Agilent system [32,24]. One of the important points is that we have replaced the thermal noise with white nose in our formulas. On the contrary, as the phenomenon of noise is heavily related to the frequency, our results have this limitation.

Also, we should note that every part of the sensor system plays a part in calculating the overall result. Having said that, any calibration of the arrangement under a defined mechanism becomes a rigorous process to ascertain accuracy and reliability in attaining the result [37,54]. In view of this, and the fact that these phenomena do not have an observable behaviour in the sensor's anticipated performance, we are able to achieve a sufficiently reliable outcome at this level.

However, we must be aware of the principles that govern the saturation condition of the SOA [13,17,44]. Any significant alteration in the gain associated with the SOA can directly or indirectly affect the sensor's functionality and accuracy. Therefore, it is important to realize that we take these potential changes into account before proceeding to utilize the sensor in practical applications. Such careful consideration will help guarantee that our measurements and assessments remain consistent and valid under various operational conditions.

A close examination of RIN of the system without the holder, the system with the holder, and the Agilent setup has therefore been done. Under the variation of the same parameters for all the experimental setups, our comparison of RIN has shown reliable and efficient results among the described scenarios, thereby ensuring a promising sensor mechanism at a later stage.

5. Conclusion

Based on the principle of ICAS, this work deals with the integration of a sample holder in the laser based setup. The selected holder is placed after considering the feasibility of the existing system. The system was analysed with the help of light source, two lenses and corresponding fibre junctions. Based on our visionless approach, our investigation leads to a minimal loss in the existing system that is not detrimental to any measurements with the substances. The holder is placed in forward and reverse directions, with an average accuracy of ± 0.2 dB, which is within the intensity loss specified by the manufacturer. The result was consistent when the positions of the lenses were swapped, strengthening the credibility of the holder in the experimental system.

Afterwards, the spectral output of the new experimental system was thoroughly examined in comparison to that of the old one, under identical set of parameters. The intensity profiles, slope, mode spacing, intensity levels and distance from the central wavelength were explored with respect to the holder's direction and the position of the lenses. Graphical outcomes were tabulated and the outcomes were highly consistent with those for the setup without any holder in it. The difference in values ranged between -0.153 and -0.202 dBs for all the input parameters which justifies a reliable prerequisite for the sensor's performance. This investigation also uncovered signs of strong mode competition when both modes were at equilibrium, a fact that can be used and further investigated for systems with multiple wavelengths with additional equipment, as the available technical features of the current measurement devices have been exploited here.

A significant connection has been established and thoroughly observed between the two distinct modes of operation within our system and their corresponding RIN spectra. An analogous sequence of RIN results with the old and new systems (without and with the holder, respectively), is indeed a worthwhile achievement for our system, and opens vistas for a multimode system. This detailed analysis proves to be exceptionally beneficial in enhancing the application of RIN estimations within the context of our spectroscopy-based system. An interesting observation is the pronounced increase in the standard value of RIN at elevated temperatures, which suggests a marked improvement in the performance and efficiency of our system as the temperature rises. This characteristic indicates that our system can operate more effectively under higher thermal conditions, making it attractive for various applications (such as [4,5,7,40]).

5.1. Considerations and insights for future work

In view of the amendments in the experimental setup, it is important to highlight that the system we have developed demonstrates the capability to achieve results that are as reliable and accurate as those previously obtained, without the holder. This equivalency underscores the effectiveness of our design and reinforces the credibility of our findings. The cost-effective nature of our apparatus is particularly noteworthy, as it makes advanced spectroscopy accessible to a broader audience. This accessibility is particularly relevant given the intended application of our system as a biomedical sensor, which has the potential to benefit a wide range of fields including medical diagnostics, research, and healthcare [1,2,8,20]. By providing a more affordable alternative, we aim to democratize the use of advanced spectroscopic techniques, ultimately fostering innovation and improving outcomes in biomedical applications.

The efficiency is expected to be enhanced by engaging an amplifier with reduced noise level. Additionally, we are thinking about supplementing the measurement system with a customized tunable laser along with its respective attenuator. Besides, negotiations are underway to examine the steadiness of the modes in defined time frames [39]. This is crucial to the system as it must consistently maintain both modes, which is fundamental to the overall concept of the biomedical device, thus ensuring the sensitivity of the anticipated sensor.

CRediT authorship contribution statement

Walaa Alayed: Data curation, Formal analysis, Funding acquisition, Investigation, Writing – original draft, Writing – review & editing. **Momna Ikram:** Conceptualization, Data curation, Formal analysis, Investigation, Project administration, Supervision, Writing – original draft, Writing – review & editing. **Usman Masud:** Conceptualization, Data curation, Formal analysis, Investigation, Methodology, Supervision, Writing – original draft, Writing – review & editing.

Funding

This research was funded by Princess Nourah bint Abdulrahman University Researchers Supporting Project number (PNURSP2025-R500), Princess Nourah bint Abdulrahman University, Riyadh, Saudi Arabia.

Declaration of competing interest

The authors declare that they have no known competing financial interests or personal relationships that could have appeared to influence the work reported in this paper.

Acknowledgements

The authors would like to acknowledge Princess Nourah bint Abdulrahman University Researchers Supporting Project number (PNURSP2025R500), Princess Nourah bint Abdulrahman University, Riyadh, Saudi Arabia for supporting this project.

Data availability

The datasets used and/or analysed during the current study available from the corresponding author on reasonable request.

References

[1] P. Sukul, J.K. Schubert, K. Zanaty, et al., Exhaled breath compositions under varying respiratory rhythms reflects ventilatory variations: translating breathomics towards respiratory medicine, Sci. Rep. 10 (2020) 14109, https://doi.org/10.1038/s41598-020-70993-0.
[2] O. Lawal, W.M. Ahmed, T.M.E. Nijsen, R. Goodacre, S.J. Fowler, Exhaled breath analysis: a review of 'breath-taking' methods for off-line analysis, Metabolomics 13 (10) (2017) 110, https://doi.org/10.1007/s11306-017-1241-8. Epub 2017 Aug 19. PMID: 28867989; PMCID, PMC5563344.
[3] Samah F. Al-Shatnawi, Karem H. Alzoubi, Rawand A. Khasawneh, Omar F. Khabour, Basima A. Almomani, Exception from informed consent for biomedical research in emergency settings: a study from Jordan, Heliyon (ISSN 2405-8440) 7 (12) (2021) e08487, https://doi.org/10.1016/j.heliyon.2021.e08487.
[4] T.A. Popov, Human exhaled breath analysis, Ann. Allergy Asthma Immunol. 106 (6) (2011 Jun) 451–456, https://doi.org/10.1016/j.anai.2011.02.016, quiz 457. Epub 2011 Apr 8. PMID: 21624743.
[5] J. Herbig, M. Müller, S. Schallhart, T. Titzmann, M. Graus, A. Hansel, On-line breath analysis with PTR-TOF, J. Breath Res. 3 (2) (2009) 027004.
[6] U. Masud, Investigations on Highly Sensitive Optical Semiconductor Laser Based Sensorics for Medical and Environmental Applications: "The Nanonose", Kassel University Press, ISBN 3862195554, 19 Jan 2015.
[7] M. Phillips, R.N. Cataneo, C. Saunders, P. Hope, P. Schmitt, J. Wai, Volatile biomarkers in the breath of women with breast cancer, J. Breath Res. 4 (2) (2010) 026003.
[8] W. Miekisch, J.K. Schubert, G.F. Noeldge-Schomburg, Diagnostic potential of breath analysis—focus on volatile organic compounds, Clin. Chim. Acta 347 (1–2) (2004) 25–39.
[9] K.M. Hangos, J. Bokor, G. Szederkényi, Analysis and Control of Nonlinear Process Systems, Springer Science & Business Media, 2006.
[10] M. Kaloumenou, E. Skotadis, N. Lagopati, E. Efstathopoulos, D. Tsoukalas, Breath analysis: a promising tool for disease diagnosis—the role of sensors, Sensors 22 (2022) 1238, https://doi.org/10.3390/s22031238.
[11] H.S.A. Grants, Provisional authorisation for 'BreFence go COVID-19 breath test system' and 'traciex breathalyser' for detection of COVID-19 infection, available online: https://www.hsa.gov.sg/announcements/regulatory-updates/hsa-grants-provisional-authorisation-for-brefence-go-covid-19-breath-test-system-and-traciex-breathalyser-for-detection-of-covid-19-infection. (Accessed 20 August 2024).
[12] MingXuan Li, HongDian Li, HongXu Liu, XiaoLei Lai, Wenlong Xing, JuJu Shang, Effect of traditional Chinese medicine cutaneous regions therapy as adjuvant treatment of chronic heart failure: a systematic review and meta-analysis, Heliyon (ISSN 2405-8440) 9 (5) (2023) e16012, https://doi.org/10.1016/j.heliyon.2023.e16012.
[13] V.M. Baev, J. Eschner, E. Paeth, et al., Intra-cavity spectroscopy with diode lasers, Appl. Phys. B 55 (1992) 463–477, https://doi.org/10.1007/BF00332504.
[14] U. Masud, F. Jeribi, A. Zeeshan, A. Tahir, M. Ali, Highly sensitive microsensor based on absorption spectroscopy: design considerations for optical receiver, IEEE Access 8 (2020) 100212–100225, https://doi.org/10.1109/ACCESS.2020.2996973.
[15] V.M. Baev, P.E. Toschek, Sensitivity limits of laser intracavity spectroscopy, in: H. Schiff, U. Platt (Eds.), Society of Photo-Optical Instrumentation Engineers (SPIE) Conference Series, in: Society of Photo-Optical Instrumentation Engineers (SPIE) Conference Series, vol. 1715, February 1993, pp. 381–392.
[16] A. Champagne, M. Lestrade, J. Camel, R. Maciejko, B. Tromborg, Degradation of side-mode suppression ratio in a DFB laser integrated with a semiconductor optical amplifier, IEEE J. Quantum Electron. 40 (7) (July 2004) 871–877, https://doi.org/10.1109/JQE.2004.830175.
[17] A. Einstein, Grundgedanken der allgemeinen Relativitatstheorie und Anwendung dieser Theorie in der Astronomie, Preuss. Akad. Wiss. Sitz.ber. 315 (1915) 778–786.
[18] A.J. Ward, et al., Widely tunable DS-DBR laser with monolithically integrated SOA: design and performance, IEEE J. Sel. Top. Quantum Electron. 11 (1) (Jan.-Feb. 2005) 149–156, https://doi.org/10.1109/JSTQE.2004.841698.
[19] Y. Posudin, Methods of analysis of volatile organic compounds, in: Y. Posudin (Ed.), Methods of Measuring Environmental Parameters, 2014.
[20] W. Demtroder, Experimentalphysik 3: Atome, Molekule und Festkorper, 3., uberarb. aufl. edition, Springer-Lehrbuch, Springer, April 2005 (German Edition).
[21] B. Van Zeghbroeck, Principles of Semiconductor Devices, University of Colorado, 2007.
[22] Zhenyang Gao, Lei Wang, Jian-Jun He, Mode competition analysis in dual-wavelength coupled-cavity semiconductor laser, J. Opt. Soc. Am. B 27 (2010) 432–441.
[23] Juhi Jannat Mim, Mehedi Hasan, Md Shakil Chowdhury, Jubaraz Ghosh, Md Hosne Mobarak, Fahmida Khanom, Nayem Hossain, A comprehensive review on the biomedical frontiers of nanowire applications, Heliyon (ISSN 2405-8440) 10 (8) (2024) e29244, https://doi.org/10.1016/j.heliyon.2024.e29244.
[24] U. Masud, M.R. Amirzada, H. Elahi, F. Akram, A. Zeeshan, Y. Khan, M.K. Ehsan, M.A. Qureshi, A. Ali, S. Nawaz, et al., Design of two-mode spectroscopic sensor for biomedical applications: analysis and measurement of relative intensity noise through control mechanism, Appl. Sci. 12 (2022) 1856, https://doi.org/10.3390/app12041856.
[25] Beer, Bestimmung der Absorption des rothen Lichts in farbigen Flüssigkeiten, Ann. Phys. 162 (1852) 78–88, https://doi.org/10.1002/andp.18521620505.
[26] Inphenix Semiconductor Optical Amplifier, Inphenix, Inc. 250 North Mines Rd, Livermore, CA 94551 USA, https://www.inphenix.com/en/semiconductor-optical-amplifiers/ (visited on September 1, 2023 - 1520 GMT).
[27] LDC-3900 ILX lightwave laser diode controller, https://www.newport.com/p/LDC-3900-120V.
[28] Advanced Optics Solutions GmbH, Overbeckstr 39a D-01139 Dresden, https://www.aos-fiber.com/eng/Company.html (visited on August 12, 2023 - 0223 GMT).
[29] Rohde & Schwarz signal and spectrum analyzer, https://www.rohde-schwarz.com/us/products/test-and-measurement/signal-and-spectrum-analyzers_63665.html (visited on August 12, 2023 - 0224 GMT).
[30] Tektronix electrical spectrum analyzer, https://www.tek.com/en/products/spectrum-analyzers (visited on August 12, 2023 - 0225 GMT).
[31] Lecroy oscilloscope, https://www.teledynelecroy.com/wr9000/ (visited on August 12, 2023 - 0227 GMT).
[32] U. Masud, M.I. Baig, Investigation of cavity length and mode spacing effects in dual-mode sensor, IEEE Sens. J. 18 (7) (1 April, 2018) 2737–2743, https://doi.org/10.1109/JSEN.2017.2788359.
[33] Ieva Uoginte, Agne Vailionyte, Martynas Skapas, Dave Bolanos, Ernesta Bagurskiene, Vygantas Gruslys, Rūta Aldonyte, Steigvile Bycenkiene, New evidence of the presence of micro- and nanoplastic particles in bronchioalveolar lavage samples of clinical trial subjects, Heliyon (ISSN 2405-8440) 9 (9) (2023) e19665, https://doi.org/10.1016/j.heliyon.2023.e19665.
[34] Alina Gearba, Gabriela Cone, Numerical analysis of laser mode competition and stability, Phys. Lett. A (ISSN 0375-9601) 269 (2–3) (2000) 112–119, https://doi.org/10.1016/S0375-9601(00)00245-0.
[35] Bruno da Silva Falcão, Ausama Giwelli, Melissa Nogueira Kiewiet, Stephen Banks, George Yabesh, Lionel Esteban, Leigh Kiewiet, Nurudeen Yekeen, Yevhen Kovalyshen, Ludwig Monmusson, Ahmed Al-Yaseri, Alireza Keshavarz, Stefan Iglauer, Strain measurement with multiplexed FBG sensor arrays: an experimental investigation, Heliyon (ISSN 2405-8440) 9 (8) (2023) e18652, https://doi.org/10.1016/j.heliyon.2023.e18652.
[36] M. Shtaif, G. Eisenstein, Noise properties of nonlinear semiconductor optical amplifiers, Opt. Lett. 21 (22) (1996) 1851–1853.
[37] David Dahan, Gadi Eisenstein, The properties of amplified spontaneous emission noise in saturated fiber Raman amplifiers operating with CW signals, Opt. Commun. (2004) 279–288.
[38] Synthetic Quartz Glass Cuvettes with Septum Screw Caps, 2 Polished Sides, https://www.thorlabs.com/newgrouppage9.cfm?objectgroup_id=5943 (visited on March 2, 2024 - 0336 GMT).

[39] S. Valentin, J. Shrestha, private communication.
[40] F. Guder, A. Ainla, J. Redston, B. Mosadegh, A. Glavan, T.J. Martin, G.M. Whitesides, Paper-based electrical respiration sensor, Angew. Chem., Int. Ed. 55 (2016) 5727, https://doi.org/10.1002/anie.201511805.
[41] SWIR EMITTER 1550NM 3MM PLASTIC, Infrared (IR) Emitter 1550nm 0.93V 100mA 240° Radial, Marktech Optoelectronics MTE5115C2, DigiKey Part Number 1125-1484-ND, https://www.digikey.com/en/products/detail/marktech-optoelectronics/MTE5115C2/9955412?s=N4IgTCBcDaILIBUCiBWAjGlBhCBdAvkA (visited on February 16, 2024 - 1224 GMT).
[42] 3-Pad LED Flip Chip COB, LED professional - LED Lighting Technology, Application Magazine, https://www.led-professional.com/resources-1/articles/3-pad-led-flip-chip-cob (visited on February 15, 2024 - 0133 GMT).
[43] Liang Sheng, Zhigang Yang, Hui Wang, Baibing Li, Xiaofen Zhang, Yunhai Jia, Analysis of Ti-inclusions in high carbon chromium bearing steel by laser-induced breakdown spectroscopy, Heliyon (ISSN 2405-8440) 9 (6) (2023) e17165, https://doi.org/10.1016/j.heliyon.2023.e17165.
[44] D. Marcuse, Loss analysis of single-mode fiber splices, Bell Syst. Tech. J. 56 (5) (May-June 1977) 703–718, https://doi.org/10.1002/j.1538-7305.1977.tb00534.x.
[45] J.M. Nichols, J.V. Michalowicz, F. Bucholtz, Distribution of splice loss in single mode optical fiber, Appl. Opt. 57 (2018) 1140–1150.
[46] Rongqing Hui, Chapter 8 - Optical transmission system design, in: Rongqing Hui (Ed.), Introduction to Fiber-Optic Communications, Academic Press, ISBN 9780128053454, 2020, pp. 337–416.
[47] Haiyan Wang, Xiuquan Li, Linqi Jin, Guijun Hu, Evaluation of splicing quality in few-mode optical fibers, Opt. Commun. (ISSN 0030-4018) 507 (2022) 127596, https://doi.org/10.1016/j.optcom.2021.127596.
[48] Radhakrishnan Nagarajan, John E. Bowers, Chapter 3 - High-Speed Lasers, in: Eli Kapon (Ed.), Optics and Photonics, Semiconductor Lasers I, Academic Press, ISBN 9780123976307, 1999, pp. 177–290, ISSN 15575837.
[49] Hua Wang, Yuxin Lei, Qiang Cui, Siqi Li, Xin Song, Yongyi Chen, Lei Liang, Peng Jia, Cheng Qiu, Yue Song, Yubing Wang, Yiran Hu, Li Qin, Lijun Wang, Noise characteristics of semiconductor lasers with narrow linewidth, Heliyon (ISSN 2405-8440) 10 (20) (2024) e38586, https://doi.org/10.1016/j.heliyon.2024.e38586.
[50] Rick Bitter, Taqi Mohiuddin, Matt Nawrocki, LabVIEW Advanced Programming Techniques, CRC Press Taylor & Francis Group, NW, 2007.
[51] Govind P. Agrawal, Niloy K. Dutta, Semiconductors Lasers, Van Nostrand Reinhold, New York, 1993.
[52] Matthew Otis, GPIB Communication, Texas A & M University.
[53] S.B. Felch, R. Brennan, S.F. Corcoran, G. Webster, A comparison of three techniques for profiling ultra-shallow p+–n junctions: greater silicon valley implant users' group, in: D.F. Downey, M. Farley, K.S. Jones, G. Ryding (Eds.), Ion Implantation Technology–92, Elsevier, ISBN 9780444899941, 1993, pp. 156–159.
[54] U. Masud, M.I. Baig, Multimode competition in lasers in the light of optical feedback, in: 2012 10th International Conference on Frontiers of Information Technology, Islamabad, Pakistan, 2012, pp. 243–247.
[55] Moustafa Ahmed, Safwat W.Z. Mahmoud, Minoru Yamada, Numerical analysis of optical feedback phenomenon and intensity noise of fibre-grating semiconductor lasers, Int. J. Numer. Model. 20 (3) (2007) 117–132, https://doi.org/10.1002/JNM.639.
[56] L.N. Langley, K.A. Shore, Jesper Mørk, Dynamical and noise properties of laser diodes subject to strong optical feedback, Opt. Lett. 19 (24) (1994) 2137–2139, https://doi.org/10.1364/OL.19.002137.
[57] Usman Masud, Mudassar Ali, Farhan Qamar, Ahmed Zeeshan, Momna Ikram, Dual mode spectroscopuc biomedical sensor: technical considerations for the wireless testbed, Phys. Scr. (10 September 2020), https://iopscience.iop.org/article/10.1088/1402-4896/abb49c/meta.
[58] Kakiuchida Hiroshi, Ohtsubo Junji, Characteristics of a semiconductor laser with external feedback, IEEE J. Quantum Electron. 30 (9) (1994) 2087–2097, https://doi.org/10.1109/3.309866.